water

MDPI

Article

Chemical-Free Regeneration of Scaled Capacitive Deionization Electrodes Using Alternating Polarization

Yazeed Algurainy

Department of Civil Engineering, College of Engineering, King Saud University, P.O. Box 2454, Riyadh 11451, Saudi Arabia; yalgurainy@ksu.edu.sa

Abstract

Mineral scaling on carbon electrodes remains a critical limitation to the long-term performance of capacitive deionization (CDI) systems treating hard and alkaline waters. In this study, alternating polarization (AP) is investigated as an in situ electrochemical regeneration strategy to reverse cathodic scaling in flow-through CDI treating a feed containing 5 mM NaCl, 5 mM $NaHCO_3$, and 2.5 mM $CaCl_2$ under three modes: conventional cycling (control), delayed AP introduced after fouling developed, and immediate AP implemented from the first cycle. Under conventional operation, cathodic scaling reduced the salt adsorption capacity (SAC) to 5.9 ± 0.2 mg/g, increased cathode mass from 0.208 ± 0.004 g (pristine) to 0.353 ± 0.054 g, and decreased specific capacitance to 28 ± 2 F/g, accompanied by extensive pore blockage and carbonate deposition observed by SEM and BET measurements. Application of delayed AP restored electrode functionality, increasing SAC to 8.9 ± 0.6 mg/g and specific capacitance to 56 ± 2 F/g while reducing the cathode mass to 0.212 ± 0.007 g and removing surface precipitates. The immediate AP operation reduced the extent of scale formation from cycle 1, maintaining SAC at 8.4 ± 0.2 mg/g throughout operation, with stable physical and electrochemical properties. These improvements are attributed to periodic polarity reversal, which induces alternating alkaline and acidic microenvironments at the electrode surface and promotes the electrochemical dissolution of carbonate phases during anodic polarization. Overall, this work establishes AP as a simple, chemical-free operational strategy for both preventing and reversing cathodic mineral scaling, thereby enabling sustained CDI performance and mitigating capacity loss over the tested operational periods in complex water matrices.

Keywords: capacitive deionization; alternating polarization; electrochemical regeneration; cathodic mineral scaling; carbonate precipitation

Check for updates

Academic Editor: Alexandre T. Paulino

Received: 26 April 2026
Revised: 8 June 2026
Accepted: 17 June 2026
Published: 19 June 2026

Copyright: © 2026 by the author. Licensee MDPI, Basel, Switzerland. This article is an open access article distributed under the terms and conditions of the Creative Commons Attribution (CC BY) license.

1. Introduction

The limited availability of freshwater resources has increased interest in technologies capable of treating low to medium salinity waters such as brackish groundwater, industrial process water, and reclaimed wastewater [1–3]. While seawater reverse osmosis and thermal desalination technologies are highly effective for seawater treatment, they are often unnecessarily energy-intensive when applied to low-to-medium salinity waters such as brackish groundwater or reclaimed wastewater [4–6]. This has motivated the development of alternative, energy-efficient electrochemical approaches for selective ion removal [7,8]. Capacitive deionization (CDI) is an electrochemical-based approach to water desalination and nutrients recovery that has gained a large attention over the last decade for its low energy consumption and simple operation [9–11]. In contrast to traditional techniques like

reverse osmosis (RO) or thermal-based systems, CDI employs an electrostatic mechanism to extract dissolved salts from water and ion storage within the electrical double layers (EDLs) of electrodes [12–14]. Upon application of an external electric potential (the charging phase), positively charged ions (cations) are attracted by the cathode, while negatively charged ions (anions) move toward the anode. During the discharging phase, the electrodes are regenerated and the adsorbed ions are typically released back into the solution. This ion separation enables efficient removal of salts, making CDI especially suitable for treating low to medium salinity water sources, including brackish groundwater [15,16].

Despite its potential, one of the main obstacles to the broader implementation of CDI in water treatment is the formation of solids (scaling) on electrode surfaces [17–19]. This issue involves the accumulation of inorganic precipitates such as calcium carbonate ($CaCO_3$), magnesium hydroxide ($Mg(OH)_2$), and calcium sulfate ($CaSO_4$) on the electrodes during operation [20]. While analogous to scaling challenges observed in conventional water treatment processes, this phenomenon introduces specific complications within CDI systems [17]. First, scale buildup reduces the electrodes' effective surface area, which is critical for ion adsorption within EDLs during the charging cycle, thus diminishing salt removal capacity [20]. Second, the presence of these deposits increases the internal resistance of the electrodes, hindering charge transfer and raising the energy demand for equivalent desalination output [21,22]. Third, scale formation can obstruct the porous network of the electrodes, restricting water flow and ion transport to active sites [20,23]. Lastly, managing the deposition of precipitates on carbon often requires periodic cleaning or electrode replacement, leading to more frequent maintenance and elevated operational expenses [24].

Scaling in CDI systems arises from multiple factors that lead to the crystallization and accumulation of poorly soluble salts on electrode surfaces. These factors are largely determined by the chemical characteristics of the feedwater, the operational parameters of the system, and the physical and chemical properties of the electrode materials. One primary contributor is the localized increase in pH resulting from electrochemical processes at the electrodes, particularly those involving oxygen reduction reactions (ORRs) at the cathode, which elevate the pH in the cathode vicinity [25–28]. Alkaline conditions promote the formation of precipitates locally [29–31]. Additionally, during ion adsorption in the charging phase, ions migrate toward the electrodes, creating a concentration gradient near the surface. This localized ion buildup may drive certain species past their solubility limits, resulting in the formation of solid deposits on the electrodes [22,32]. The extent of scaling is further influenced by system variables such as voltage, water flow rate, and electrode characteristics [33,34]. Particularly, feedwaters with elevated levels of divalent cations like Ca^{2+} and Mg^{2+} present a higher risk for scale development due to their tendency to form insoluble compounds that quickly accumulate on electrode surfaces [20,35].

Preventing scale buildup is essential to ensure sustained performance and to minimize operational issues associated with maintenance or electrode replacement [36]. A range of strategies has been investigated, particularly those involving modifications to electrode materials and adjustments to system operating parameters. With regard to material-based approaches, charged surface coatings or functional layers deposited directly onto carbon electrodes primarily act at the electrode–electrolyte interface, where they modify local electrostatic interactions, ion partitioning, and transport kinetics [37–40]. By altering the local environment at reactive sites, these layers can reduce the accumulation of divalent scaling ions such as Ca^{2+} at high-pH regions, thereby mitigating nucleation and surface precipitation without necessarily preventing overall ion removal [41,42]. Moreover, ion-selective layers such as ion-exchange membranes placed over electrodes as macroscopic transport barriers that regulate ionic flux based on charge and valence, thereby controlling the exposure of the carbon surface to divalent species and enabling selective ion transport

and scaling suppression [43–46]. On the operational side, optimizing variables such as applied voltage and cycling protocols can help regulate local pH shifts near the electrodes, thereby limiting highly alkaline microenvironments and the associated formation of sparingly soluble precipitates [47,48]. Lower operating voltages are widely used in CDI to reduce faradaic side reactions such as hydroxide generation, which otherwise intensify with increased potential and raise local supersaturation risk under alkaline conditions [49–52].

Moreover, alternating polarization (AP), i.e., the periodic reversal of electrode polarity, has been explored to improve electrode durability under prolonged cycling conditions. Earlier investigations into AP primarily focused on its application for mitigating anodic carbon corrosion; by reversing polarity, these systems successfully limit continuous oxidation and degradation at the anode surface [53–56]. However, while AP is established as a strategy for anodic preservation, its potential to actively manage and reverse cathodic mineral scaling, which is a fundamentally distinct electrochemical challenge, has not yet been systematically explored.

Building upon these foundational AP studies, the present work investigates AP as an in situ electrochemical regeneration strategy for fouled cathodes in scaling-prone feedwaters containing Ca^{2+} and HCO_3^-. The hypothesis here is that periodic polarity reversal induces alternating alkaline and acidic microenvironments, where the transient anodic polarization of the former cathode generates localized protons (via carbon oxidation) that facilitate the dissolution of carbonate-based precipitates. Therefore, this study distinguishes itself by shifting the application of AP from anodic corrosion mitigation to cathodic scale dissolution, providing mechanistic insights into scale dynamics under dynamic polarization and establishing a chemical-free approach for maintaining electrode functionality. To test this hypothesis, a flow-through CDI cell was operated under three scenarios: (i) a conventional cycling mode serving as the control, in which persistent cathodic scaling was expected; (ii) a delayed regeneration mode, in which AP was applied after scaling had developed; and (iii) an immediate regeneration mode, in which AP was applied from the first cycle to inhibit scale formation. The electrode morphology, pore structure, and electrochemical behavior were characterized using scanning electron microscopy (SEM), N_2 sorption analysis, and cyclic voltammetry (CV), and desalination performance was quantified using salt adsorption capacity (SAC) derived from desorption profiles. This work demonstrates that AP can serve not only as a preventive strategy but also as an effective electrochemical regeneration mechanism for reversing cathodic mineral scaling in CDI systems, providing mechanistic insight into scale formation and dissolution under dynamic polarization and establishing AP as a simple, chemical-free approach for maintaining electrode functionality in scaling-prone water matrices.

2. Methodology

2.1. Cell Assembly and Conditioning

A symmetric flow-through capacitive deionization (FT-CDI) cell was assembled using two identical activated carbon cloth (ACC-5092-15, Nippon Kynol, Osaka, Japan), each with 3 cm diameter, 0.5 mm thickness, specific surface area approximately 1500 m^2/g, and a dry mass of 0.2 g. This ACC was selected for its high surface area, well-developed pore structure, and favorable electrical conductivity, which together enhance electrosorption capacity and charge transfer efficiency [33]. Each electrode was attached to a graphite current collector (5 cm × 5 cm × 0.1 cm) to ensure low contact resistance and stable electrical connectivity, with a 3 cm diameter central opening to permit water flow. A non-conductive polypropylene spacer (3501, Celgard, Charlotte, NC, USA) with 0.45 μm pore size was positioned between the electrodes to maintain separation and facilitate uniform electrolyte flow through the porous structure. The assembly was housed within

a rigid polycarbonate frame, with stainless steel plates and screws providing mechanical stability and consistent compression during operation [30]. The fully assembled cell was connected to a peristaltic pump (Masterflex, Cole-Parmer, Vernon Hills, IL, USA), which supplied feedwater at a constant flow rate of 3 mL/min in a single-pass configuration. This operational mode was chosen to simulate continuous-flow conditions commonly encountered in practical CDI systems, enabling direct comparison with previous studies on flow-through architectures [57–59].

New ACC electrodes were used for each CDI test to minimize interference from previous experiments and prevent irreversible reactions. Prior to experimental use, electrodes were rinsed thoroughly with deionized (DI) water and subsequently soaked for at least 24 h to allow removal of surface-bound dust and soluble contaminants, a standard practice reported to enhance reproducibility and prevent premature fouling [60–62].

2.2. Feedwater Composition

The feedwater was prepared using DI water with a resistivity of 18 MΩ·cm (Purelab Quest, Veolia, Riyadh, Saudi Arabia). The synthetic solution contained three salts: NaCl (5 mM; >99% pure, Fisher Scientific, Waltham, MA, USA), serving as the background electrolyte to facilitate electrosorption; $NaHCO_3$ (5 mM; >99% pure€), providing bicarbonate ions; and $CaCl_2$ (2.5 mM; USP Grade, RPI, Mount Prospect, IL, USA), serving as the calcium source. These concentrations were selected to mimic the ionic composition of typical brackish waters and are consistent with values reported in the CDI literature [63,64]. The prepared solution had a conductivity of approximately 1500 µS/cm and a pH of 8.11. No visible $CaCO_3$ precipitation was observed in the feedwater prior to experiments, ensuring that any precipitate formation detected on the electrode surface would solely result from voltage applications and electrochemically induced reactions during CDI operation. For all experiments, fresh feedwater was used to maintain identical inlet chemistry throughout the charging and discharge cycles.

2.3. CDI Operation and Voltage Control

The CDI cell was operated in constant-voltage mode using a potentiostat (VSP, Bio-Logic, Seyssinet-Pariset, France). During the charging phase, a cell voltage of 1.2 V was applied across the electrodes for 30 min, followed by a 30 min discharge phase at 0 V, resulting in a cycle duration of 60 min. This operating voltage was selected to balance high electrosorption capacity while avoiding the excessive Faradaic side reactions and extreme pH shifts that are typically exacerbated at higher potentials. Each experimental run consisted of 16 consecutive cycles. This specific timeframe was selected to isolate the scaling and regeneration mechanisms. Operating the system for extended periods often introduces confounding variables, particularly progressive carbon oxidation and structural degradation at the anode. By limiting the operational duration, the specific impacts of AP on calcium carbonate precipitation and dissolution could be evaluated without interference from long-term material deterioration. Operation under this conventional 1.2 V/0 V charging–discharging protocol served as the control condition in this study.

Regeneration using AP was evaluated under two scenarios. In the first scenario, AP was applied after conventional cycling to regenerate a previously scaled cathode (denoted as delayed AP). In this mode, the first 8 cycles were operated under conventional conditions (1.2 V/0 V), followed by 8 cycles under AP, where the polarity was reversed during charging (−1.2 V/0 V), for a total of 16 cycles. In the second scenario, AP was applied from the beginning of the experiment using pristine electrodes to inhibit scale formation from the outset (denoted as immediate AP), and the cell was operated for 16 consecutive cycles with the charging polarity alternated between +1.2 V/0 V and −1.2 V/0 V in successive cycles.

All other operating conditions were kept identical across experiments to ensure a consistent basis for evaluating the influence of AP on electrode scaling and regeneration behavior.

2.4. Analytical Techniques

Effluent conductivity was monitored using an inline, flow-through conductivity sensor (ET908, eDAQ, Denistone East, NSW, Australia) positioned approximately 2 cm downstream from the cell outlet. Measurements were automatically recorded at 12 s intervals throughout operation to ensure continuous monitoring of ionic changes.

Cyclic voltammetry (CV) measurements were performed immediately after CDI cycling to evaluate the electrochemical performance of both pristine and cycled cathodes. The measurements were conducted directly in the CDI cell, operated in a two-electrode configuration with the cathode serving as the working electrode and the anode functioning simultaneously as the counter and reference electrodes. The electrolyte was identical to the feedwater composition used in the CDI experiments to ensure consistency in ionic environment. Prior to CV analysis, the cell was maintained under open-circuit conditions for at least two hours to stabilize the electrode potential, which is essential for obtaining reproducible voltammograms. CV scans were collected at least three times within a potential window of +0.5 V to −0.5 V at a scan rate of 5 mV/s. The specific capacitance (C_s) of the electrode was calculated from the CV curves (Equation (1)) to assess any changes in the capacitive behavior resulting from scaling or regeneration treatments [65,66].

$$C_s = \frac{\Delta I}{2vm} \tag{1}$$

where I represents the current, v is the scan rate (V/s), and m is the mass of the electrode (g).

Scanning electron microscopy (SEM) analysis was performed on electrodes after CDI cycling to evaluate the surface morphology of the electrodes and to assess the effectiveness of regeneration treatments. Immediately after removal from the CDI cell, electrodes were dried at 105 °C for at least 24 h without rinsing with deionized water in order to avoid unintentional removal of attached precipitates that could interfere with subsequent morphological and compositional analysis. SEM imaging was conducted using a high-resolution field emission SEM (JSM-6380 LA from JEOL, Musashino, Akishima, Tokyo, Japan) operated at an accelerating voltage of 30 kV. To characterize the elemental composition of surface deposits, energy-dispersive X-ray spectroscopy (EDS) was carried out in parallel with SEM. Multiple regions of each electrode were analyzed to account for potential spatial heterogeneity in scaling. The combined SEM–EDS approach provided complementary morphological and compositional evidence of solid precipitation and enabled assessment of its removal efficiency following the regeneration treatment processes [67–69].

Nitrogen gas sorption analysis was performed on both pristine and cycled electrodes to assess changes in their physical properties, including pore size distribution, specific surface area, and pore volume, resulting from CDI operation [70,71]. Measurements were conducted using a surface area and porosity analyzer (Autosorb iQ-x, Quantachrome, Boynton Beach, FL, USA) at 77 K. Prior to analysis, electrodes were degassed under vacuum at 350 °C for 5 h to remove adsorbed moisture and contaminants. The adsorption–desorption isotherms obtained were analyzed using non-local density functional theory (NLDFT), assuming a slit-shaped pore geometry representative of the ACC structure [72]. The total pore volume was determined from the volume of nitrogen adsorbed at a relative pressure (P/P_0) close to unity (typically 0.99), reflecting the filling of all accessible pores. Micropore surface area and micropore volume were quantified from the NLDFT pore size distribution by integrating contributions from pores smaller than 2 nm. This characterization enabled di-

rect comparison of pore structural changes induced by scaling and regeneration treatments applied during CDI cycling [22,73,74].

2.5. CDI Performance Metrics

The desalination performance of CDI cells was quantified using salt adsorption capacity (SAC), which is defined as the mass of dissolved salts removed per unit mass of active electrodes (both anode and cathode). For a single-pass, constant-flow operation, SAC was computed by integrating the concentration difference between influent and effluent over the desorption phase period according to (Equation (2))

$$\mathrm{SAC}\left(\frac{\mathrm{mg}}{\mathrm{g}-\mathrm{C}}\right) = \frac{Q * \int (C_0 - C_t)\mathrm{dt}}{m} \quad (2)$$

where Q is the volumetric flow rate (mL/min), C_0 and C_t are the influent and time-resolved effluent concentrations (mg/L), and m is the mass of both electrodes (g).

3. Results and Discussion

3.1. Desalination Performance

Effluent conductivity was monitored first as it provides direct insight into the ion removal and release dynamics of the CDI cells (Figure 1). During the charging phase of the conventional operation (control) mode (1.2 V/0 V), conductivity decreased rapidly from approximately 1.26 ± 0.01 to 0.85 ± 0.02 mS/cm, indicating a rapid onset of ion electrosorption as electric double layers formed on the electrode surfaces. The rate of decline gradually diminished and stabilized near a plateau roughly 100 µS/cm below the influent value, signifying that the electrodes approached their adsorption capacity and that mass transfer limitations began to dominate [75]. This plateau behavior suggests that a fraction of the removed ions was no longer participating in reversible electrosorption, but instead accumulated on or within the electrode as sparingly soluble mineral phases. This interpretation is supported by previous quantitative mass balance analyses under identical system conditions, which tracked calcium removal and recovery to confirm irreversible cathodic carbonate scaling [20]. During the discharging phase, the effluent conductivity exhibited a characteristic spike approximately two minutes into discharge before gradually returning to equilibrium, representing the transient release of adsorbed ions following the removal of the potential. The slight asymmetry between the charging and discharging profiles implies incomplete electrode regeneration, most likely caused by ion entrapment within blocked pores or by calcium carbonate ($CaCO_3$) deposition on the cathode surface [76].

When operated under the delayed AP mode, the effluent conductivity decreased rapidly at the beginning of the charging phase and reached approximately 0.75 ± 0.01 mS/cm, reflecting efficient ion electrosorption on the regenerated electrodes. Unlike the control test, however, the conductivity did not stabilize at a plateau but instead gradually increased toward the influent level as the cycle progressed. This behavior indicates that the electrodes initially regained high activity after polarity alternation, yet reached adsorption equilibrium more rapidly due to improved surface accessibility and ion transport kinetics [55]. The absence of a persistent conductivity offset suggests that the previous pore blockage by precipitated salts was largely alleviated following the AP operation. During discharge, the conductivity response remained qualitatively similar to the conventional mode, although the area enclosed by the conductivity curve was larger, implying greater ionic release and improved electrode regeneration efficiency.

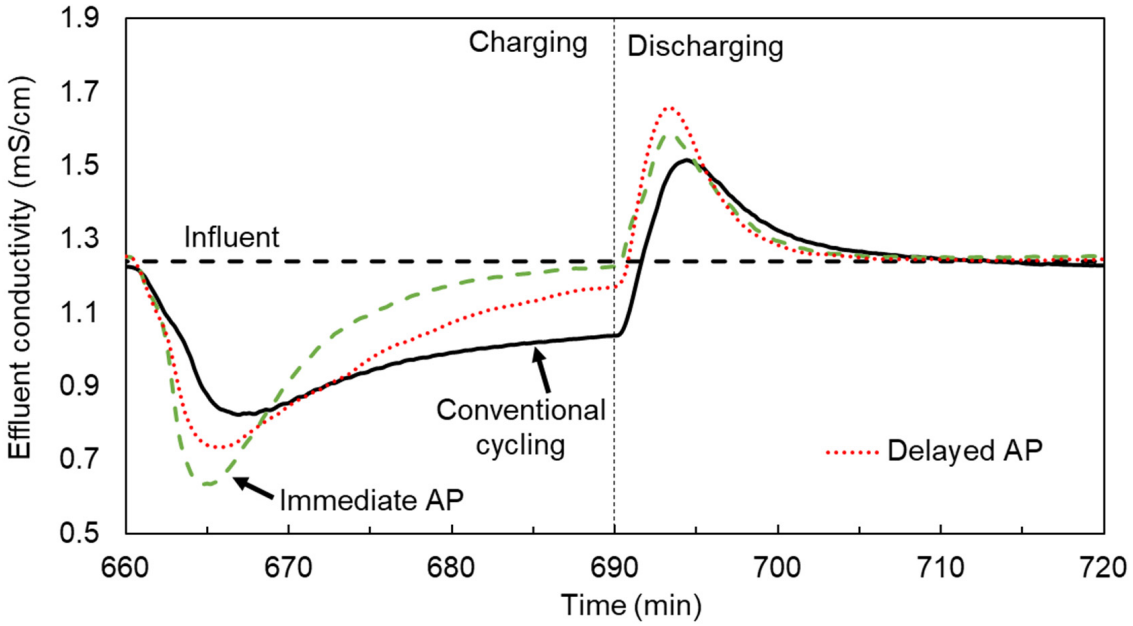


Figure 1. Effluent conductivity profiles during the charging and discharging phases under three CDI operational modes: conventional cycling (black solid line), delayed alternating polarization (AP) (red dotted line), and immediate AP (green dashed line). The horizontal dashed line shows the influent conductivity, while the vertical line indicates the transition between the charging and discharging phases.

When the cell was operated under the immediate AP mode, the effluent conductivity decreased rapidly during charging to a lower minimum of approximately 0.66 ± 0.04 mS/cm at around 5.2 min, then rose progressively toward the influent value. This deeper minimum in the present cycle indicates stronger early-cycle ion uptake relative to the control (~0.85 mS/cm) and delayed-AP (~0.75 mS/cm) modes, while the absence of an extended plateau suggests reversible adsorption without persistent transport limitation. During discharge, a transient spike slightly above the influent conductivity was observed, followed by a smooth return toward baseline. These features are consistent with polarity alternation, which mitigates local scaling effects within each cycle; however, confirmation of overall performance improvement requires quantitative evaluation using SAC.

The SAC values for all operational approaches were determined from the desorption phase to capture only the reversible portion of ion removal associated with electrosorption and exclude contributions from irreversible precipitation [77,78]. The control mode showed the lowest average SAC of 5.9 ± 0.2 mg/g-C, consistent with the limited conductivity reduction and the onset of pore blockage inferred from the plateau behavior (Figure 2). In comparison, both AP modes demonstrated substantially higher capacities. In particular, the delayed-AP mode achieved the highest SAC of 8.9 ± 0.6 mg/g-C, while the immediate-AP mode reached 8.4 ± 0.2 mg/g-C, corresponding to an improvement of roughly 40–50% over the control. The slightly higher capacity in the delayed-AP case may be attributed to partial electrode conditioning during the initial conventional cycles, which facilitated subsequent surface reactivation when polarity was reversed. These findings confirm that AP effectively restores ion-accessible surface area, mitigates scaling-induced performance loss, and enhances the reversible electrosorption behavior of the CDI system.

Overall, the conductivity and SAC results collectively demonstrate that polarity alternation improves desalination performance by preventing persistent cathodic scaling and promoting in situ electrode regeneration. The delayed-AP configuration provides evidence of performance recovery following $CaCO_3$ deposition, whereas immediate AP

offers steady operation with minimized hysteresis and stable charge/discharge symmetry. These behaviors highlight AP as a promising operational strategy for maintaining CDI efficiency in the presence of multivalent ions and carbonate alkalinity.

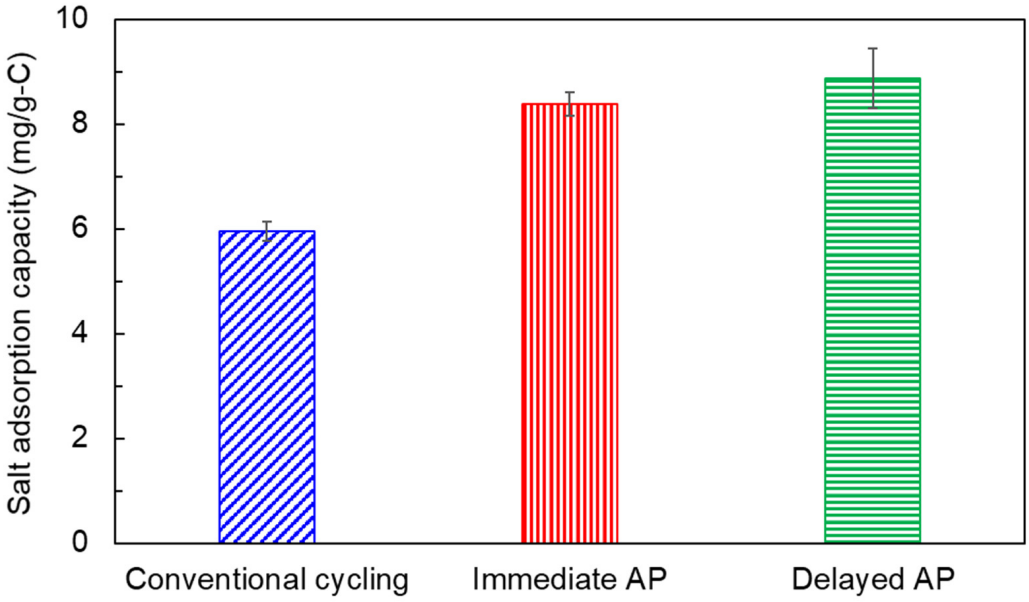


Figure 2. Salt adsorption capacity (SAC) under three CDI operational modes: conventional cycling, delayed alternating polarization (AP), and immediate AP. Error bars represent the standard deviation of triplicate measurements.

3.2. Electrode Mass Change and Scaling Suppression

To verify whether AP effectively removed surface deposits and mitigated scaling, the masses of the cathode and anode were measured before and after cycling under each operational mode (Figure 3). The pristine (pre-cycled) electrodes weighed 0.208 ± 0.004 g and served as the reference for comparison. In the control mode, the cathode mass significantly increased (0.353 ± 0.054 vs. 0.208 ± 0.004 g, $p < 0.05$), confirming substantial deposition of $CaCO_3$ crystals during conventional CDI operation, whereas the anode mass remained nearly unchanged (0.216 ± 0.008 vs. 0.208 ± 0.004 g, $p = 0.24$). This asymmetric mass gain supports the formation of precipitates primarily on the cathode, consistent with earlier evidence of $CaCO_3$ scaling in mixed Ca–HCO_3^- feedwater [20].

Following the application of AP, a significant reduction in cathode mass was observed relative to the control. The delayed and immediate AP modes resulted in cathode masses of 0.212 ± 0.007 and 0.238 ± 0.005 g, corresponding to mass reductions of 29 ± 13 and 38 ± 12%, respectively, relative to the control cathode ($p < 0.05$). These observations provide additional quantitative evidence that AP successfully removed accumulated deposits from the electrode surface. The smaller cathode masses observed under AP modes are attributed to the detachment and electrochemical dissolution of sparingly soluble salts, likely $CaCO_3$ or $Ca(OH)_2$, formed during conventional operation. Under AP, the periodic reversal of electrode polarity induces alternating alkaline and acidic microenvironments near the surface [79,80].

$$\frac{1}{4}C + \frac{1}{2}H_2O \rightarrow \frac{1}{4}CO_2 + H^+ + e^- \quad E^\circ = 0.7 - 0.9\ V/SHE \tag{3}$$

It is critical to distinguish between the short-term chemical mechanism of carbon oxidation and its long-term physical consequences. Under the applied anodic potentials, the oxidation reaction (Equation (3)) is mechanistically essential for regeneration, as it provides the localized proton release required to rapidly reverse carbonate precipitation [30]. While

prolonged carbon oxidation over extended operational lifespans would eventually lead to structural electrode degradation, the limited 16-cycle timeframe used in this study exploits the beneficial acidification for descaling without causing a detrimental loss of the carbon matrix [81]. Such cyclic acidification and neutralization behaviors have been reported to dissolve surface-bound carbonate phases without noticeably damaging the underlying carbon [82,83], which directly aligns with the stable anode masses (0.232 ± 0.017 g vs. 0.218 ± 0.014 g, $p = 0.14$) and restored capacitance observed in the present findings.

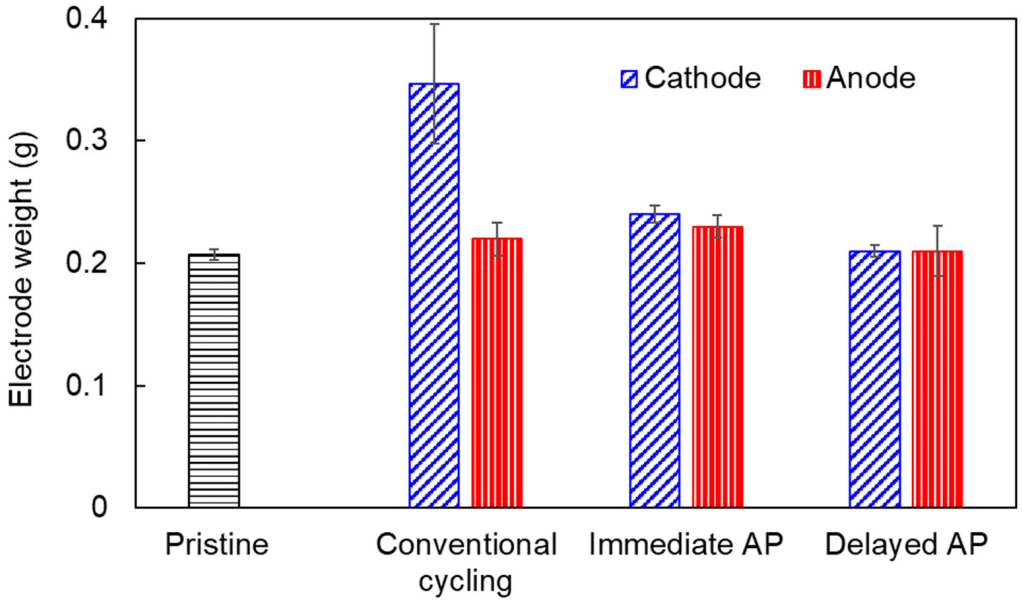


Figure 3. Electrode mass for pristine (pre-treatment) and cycled (cathode and anode) electrodes after 16 CDI cycles under three operational modes: conventional cycling, delayed alternating polarization (AP), and immediate AP. Error bars represent the standard deviation of triplicate measurements.

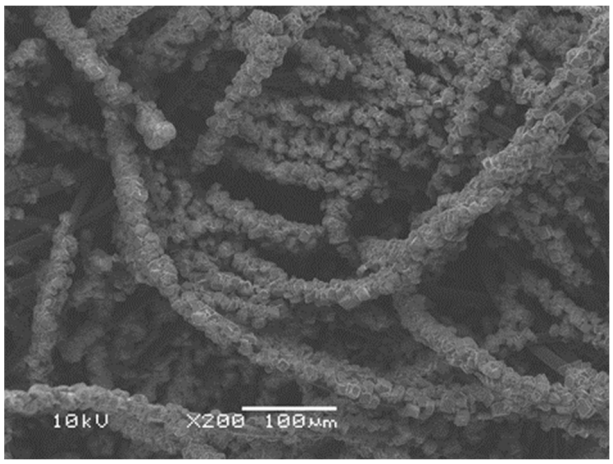
3.3. Morphological and Surface Characterization

Scanning electron microscopy (SEM) was employed to examine morphological changes in the electrodes under different polarization modes and to visually assess the impact of AP on surface scaling. The pristine electrode exhibited smooth, intertwined carbon fibers with clean surfaces and open inter-fiber channels (Figure S1), reflecting the highly porous architecture that enables efficient ion transport and adsorption.

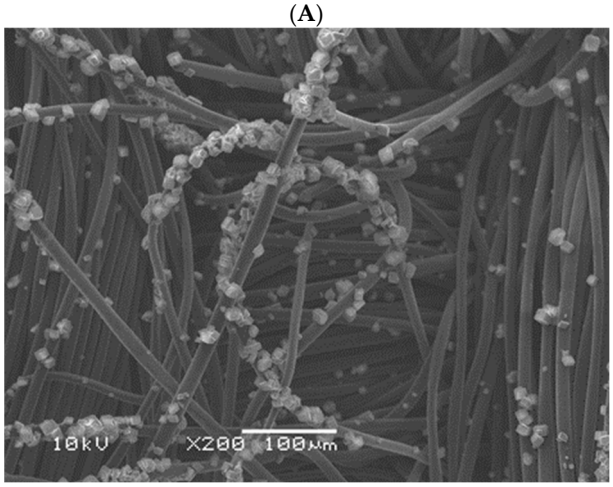
After operation in the control mode, the cathode surface became densely covered with angular and cubic crystalline aggregates that bridged adjacent fibers, forming a compact layer of mineralized deposits (Figure 4A). While EDS analysis alone cannot definitively confirm the crystallographic phase, these deposits are hypothesized to be predominantly calcium carbonate ($CaCO_3$) crystals. This assessment is strongly supported by a previous investigation utilizing the identical flow-through CDI cell and Ca–HCO_3^- feedwater chemistry, alongside the established understanding of localized pH elevation driven by cathodic reduction reactions [20,84,85]. Such deposit coverage physically blocks ion-accessible pores, which explains the increased electrode mass and diminished salt removal observed under conventional CDI cycling.

In contrast, the cathode recovered using delayed-AP operation showed a substantially cleaner morphology (Figure 4B). Most crystalline deposits were removed, and the fibrous carbon network reappeared with only minor residual particulates. This partial restoration indicates that AP effectively dissolved or detached previously accumulated scales during anodic half-cycles, when localized proton generation from carbon oxidation acidified the interface and enhanced carbonate solubility. The surface of the cathode from the immediate-

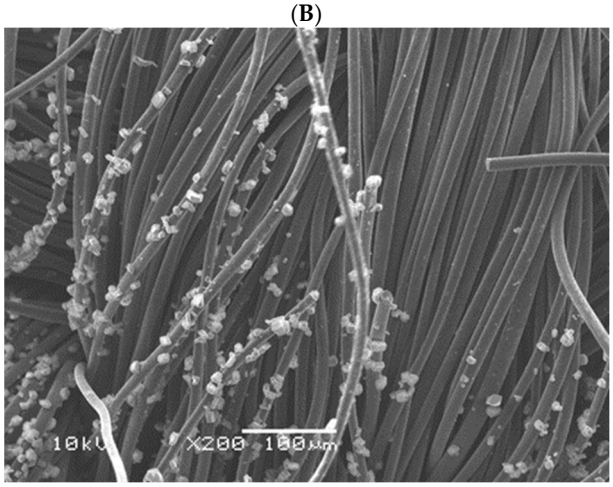
AP mode appeared even more pristine, with minimal particulate residues and fully exposed fibers (Figure 4C). This morphology closely resembled the uncycled electrode, suggesting that AP from the first cycle prevented continuous scaling rather than merely reversing it afterward.



(**A**)



(**B**)



(**C**)

Figure 4. SEM images of the cathodes after 16 CDI cycles under three operational modes: (**A**) conventional cycling, (**B**) delayed alternating polarization (AP), and (**C**) immediate AP.

The EDS spectra further corroborate the SEM observations, showing a pronounced calcium signal in the cathode operated under conventional conditions, consistent with extensive surface coverage by deposited phases (Figure S2A). In contrast, cathodes sub-

jected to delayed and immediate AP exhibited markedly reduced calcium peaks alongside dominant carbon signals, indicating partial surface coverage and effective removal of deposited species. These results confirm that AP mitigates the accumulation of carbonate-rich deposits, in agreement with the morphological evidence (Figure S2B,C).

The anodes examined after cycling under conventional and delayed AP modes remained morphologically similar to the pristine electrode, displaying smooth and nearly deposit-free surfaces (Figure S3A–C). In contrast, the anode in the immediate AP mode exhibited localized crystalline deposits, which is consistent with periodic polarity reversal where the electrode functions as a cathode during alternate cycles. This behavior confirms that precipitation is governed by cathodic conditions associated with oxygen reduction reactions (ORRs). The absence of measurable anode mass loss over 16 cycles indicates that, despite possible anodic carbon oxidation, no significant electrode consumption occurred under the tested conditions.

Overall, SEM-EDS observations provide direct morphological evidence that AP effectively mitigates mineral scaling and preserves the structural integrity of both electrodes. The progressive transition from heavy crystalline coverage in the control cathode to nearly pristine surfaces in the immediate-AP case visually supports the electrochemical and gravimetric results, confirming that AP maintains the active surface area required for sustained capacitive performance.

3.4. Electrode Pore Structure

To further quantify the impact of AP on the structural integrity and ion-accessible porosity of the electrodes, nitrogen gas sorption analyses were performed on the pristine and cycled cathodes. The pristine cathode exhibited a total pore volume (TPV) of $0.627 \pm 0.022\ cm^3/g$, with a micropore volume (MPV, $\leq$2 nm) of $0.534 \pm 0.003\ cm^3/g$ (Figure 5A). The corresponding total surface area reached $1520 \pm 10\ m^2/g$, with $1470 \pm 20\ m^2/g$ from micropores (Figure 5B). These values confirm the predominately microporous structure of the pristine carbon while highlighting the critical contribution of mesopores as ion-transport channels feeding the interior adsorption sites.

After conventional CDI operation, severe textural loss occurred. The control cathode displayed a TPV of $0.428 \pm 0.042\ cm^3/g$ and an MPV of $0.355 \pm 0.016\ cm^3/g$, indicating retention of only 68% of total and 67% of micropore volume. The total surface area of the cathode dropped to $1020 \pm 20\ m^2/g$, with $990 \pm 10\ m^2/g$ in micropores. This pronounced mesopore collapse reflects blockage by $CaCO_3$ crystallites bridging carbon fibers, consistent with the SEM-EDS results and explaining the sluggish ionic response and reduced SAC observed under the control operational mode.

The delayed-AP cathode, regenerated after initial fouling, showed a strong recovery of porosity. In particulate the electrode TPV reached $0.551 \pm 0.014\ cm^3/g$ with an MPV of $0.488 \pm 0.002\ cm^3/g$, restoring 87% of total and 92% of micropore volume. Corresponding surface areas were $1420 \pm 10\ m^2/g$ total and $1380 \pm 20\ m^2/g$ microporous. These recoveries confirm that alternating polarity cycles successfully dissolved surface-bound carbonate layers and reopened partially blocked pore entrances, restoring ion-accessible pathways.

When AP was applied from the first cycle, the immediate-AP cathode maintained nearly pristine texture. In particular, it showed a TPV of $0.532 \pm 0.008\ cm^3/g$ and MPV of $0.467 \pm 0.013\ cm^3/g$, representing 84% and 89% retention of the corresponding pristine values. The total surface area reached $1360 \pm 20\ m^2/g$, with $1320 \pm 10\ m^2/g$ in micropores. These results support the delayed AP observations and show that immediate polarity alternation effectively prevented scale accumulation on the cathode throughout cycling.

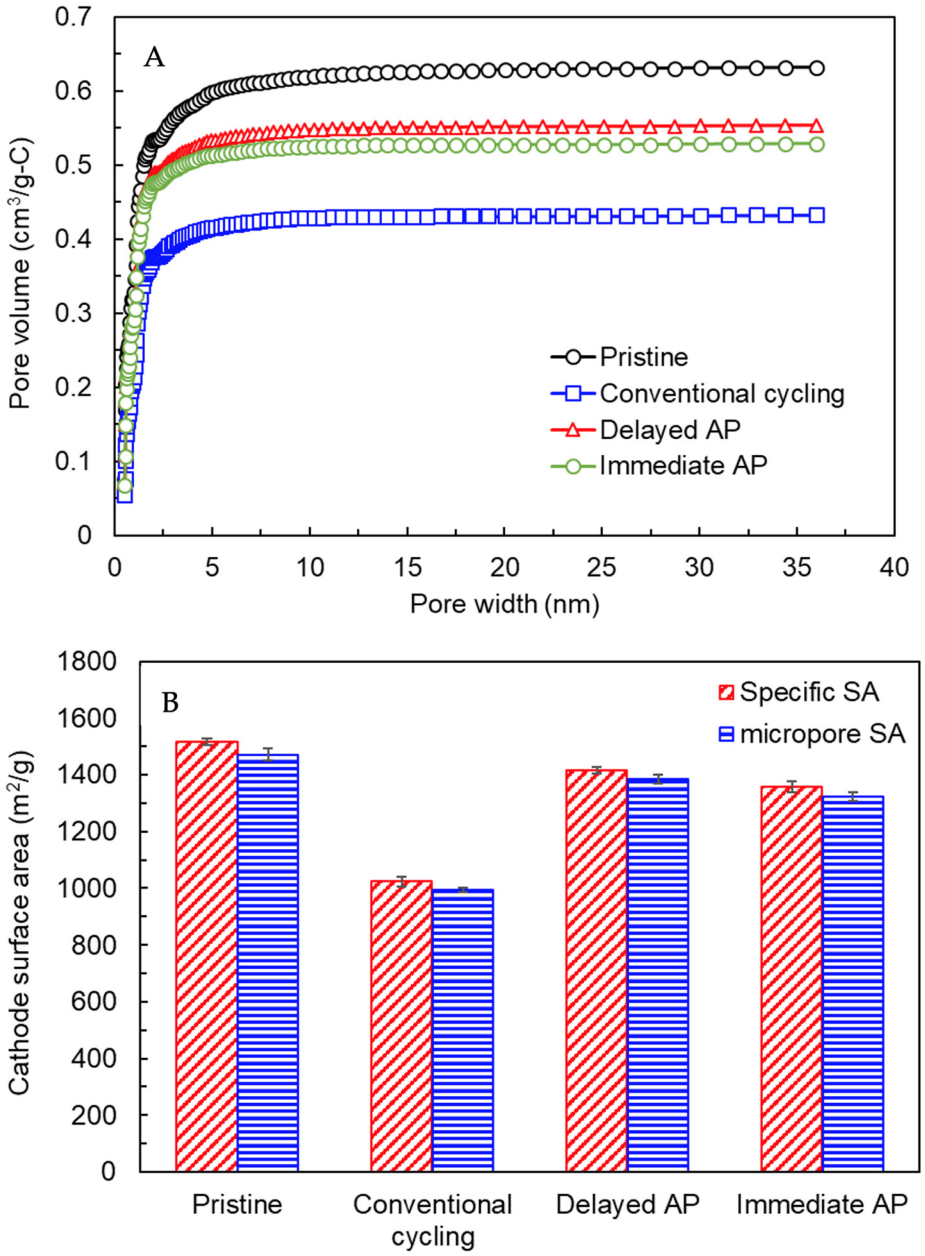


Figure 5. Pore volume (**A**) and surface area (**B**) of the pristine activated carbon (AC) electrode compared with cathodes after 16 CDI cycles under three operational modes: conventional cycling, delayed alternating polarization (AP), and immediate AP.

Collectively, the pore-volume and surface-area data corroborate the SEM and gravimetric evidence, showing that conventional CDI leads to severe mesopore occlusion and partial micropore blockage by carbonate deposits, whereas AP restores and preserves ion-accessible structure. The delayed-AP mode regenerates fouled electrodes through repeated anodic dissolution of $CaCO_3$, while the immediate-AP mode maintains open pores from the outset. These textural restorations explain the higher SAC in both AP modes relative the control mode, confirming that AP indeed enables in situ regeneration of CDI electrodes exposed to Ca–HCO_3^- feedwaters and sustains long-term electrosorption efficiency.

3.5. Electrochemical Behavior and Specific Capacitance

To evaluate the capacitive behavior and electrochemical reversibility of the cathodes after cycling under different operational modes, CV analysis was performed on a cycled cathode from each mode. The voltammograms of all electrodes displayed quasi-rectangular

shapes typical of electric double-layer capacitance in CDI electrodes [86], with no pronounced redox peaks, indicating that charge storage was predominantly capacitive and that Faradaic reactions played a limited role under the applied potential range (Figure 6). However, the area enclosed by the CV curves varied significantly among the samples, reflecting differences in accessible surface area and ionic transport pathways resulting from scaling or regeneration processes.

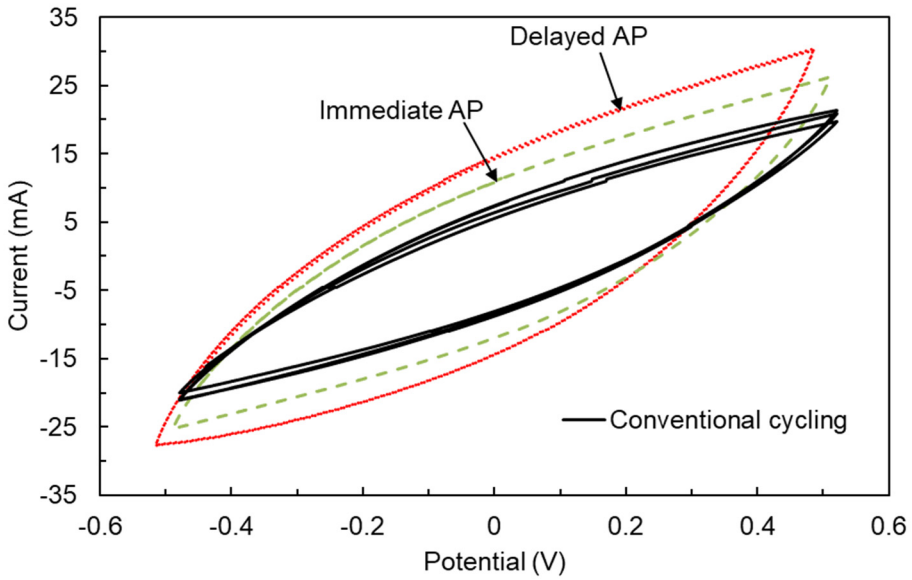


Figure 6. Cyclic voltammetry (CV) curves of the CDI cell under three operational modes: conventional cycling (black solid line), delayed alternating polarization (AP) (red dotted line), and immediate AP (green dashed line).

The control cathode showed the smallest CV area, consistent with a mean specific capacitance of 28 ± 2 F/g, confirming that carbonate scaling and pore blockage severely restricted the effective surface area for double-layer formation. This value is only 42% of the pre-cycled electrode capacitance (66 ± 1 F/g) [20], and aligns with the reduced salt adsorption capacity and the substantial loss of mesoporous structure observed in the physical analysis. The sluggish ionic response near the potential switching points further supports that ion diffusion was hindered by thick deposits, producing higher resistance and limited charge propagation through the porous network [87].

In contrast, both electrodes regenerated through AP displayed significantly enhanced capacitive performance. The delayed-AP cathode achieved the highest capacitance of 56 ± 2 F/g, nearly double that of the control. The immediate-AP mode also exhibited a markedly higher capacitance of 45 ± 1 F/g, representing a 58% improvement relative to the control.

These electrochemical trends reinforce the findings from gravimetric, SEM, and pore structure analyses that conventional CDI operation leads to severe cathodic scaling and loss of electroactive surface, whereas AP modes regenerate or preserve the electrode's capacitive functionality [88]. The increases in specific capacitance under AP operation quantitatively demonstrate the restoration of ion-accessible surface area and improved electronic connectivity within the electrode structure. Collectively, these results confirm that AP not only suppresses carbonate deposition but also sustains the electrochemical responsiveness of CDI electrodes, thereby extending their operational stability and desalination efficiency.

3.6. Future Perspectives: Coupling AP Regeneration with Resource Recovery

Beyond restoring the electrochemical performance of fouled CDI electrodes, AP introduces future opportunities to couple in situ electrode regeneration with downstream resource recovery processes. The electrochemically driven dissolution of surface-bound carbonate phases offers a controllable means of mobilizing previously precipitated calcium without external chemical dosing [89–91]. Hypothetically, this calcium-enriched effluent could be repurposed for targeted applications, such as phosphorus recovery from human urine via calcium phosphate precipitation, a process that typically requires external calcium addition [92–96]. While this study establishes the fundamental feasibility of electrochemically mobilizing precipitated species, these downstream applications remain speculative. Future investigations are required to quantify the kinetics of calcium release under varying AP conditions and to evaluate the practical integration of AP-regenerated CDI systems with downstream chemical or electrochemical nutrient capture technologies.

Moreover, while this study demonstrates the fundamental effectiveness of AP for mitigating calcium carbonate scaling, the synthetic feedwater utilized represents a simplified model. Real brackish groundwater and wastewater matrices contain a complex array of competing ions and contaminants, including magnesium, sulfate, silica, and natural organic matter. These species can precipitate as alternative scaling phases, such as magnesium hydroxide or calcium sulfate, or cause competitive adsorption and organic fouling. Therefore, the findings presented here serve as a mechanistic proof of concept. Future pilot-scale studies utilizing real water matrices are necessary to evaluate the robustness and practical deployment of AP under fully representative environmental conditions. Furthermore, subsequent research should evaluate the commercial viability, environmental implications, and broader circular economy relevance of deploying AP in scaled-up systems.

4. Conclusions

This study demonstrates that alternating polarization (AP) is an effective and robust strategy for regenerating fouled capacitive deionization (CDI) electrodes and restoring desalination performance in scaling-prone feedwaters containing Ca^{2+} and HCO_3^-.

Under conventional operation, cathodic mineral scaling led to substantial degradation of electrode function, characterized by severe pore blockage, increased electrode mass, and significantly reduced salt adsorption capacity. The application of AP effectively countered these issues. Implementing AP after fouling had developed (delayed-AP) successfully dissolved crystalline carbonate deposits, reversed pore occlusion, and restored electrochemical capacitance. Alternatively, applying AP from the first cycle (immediate-AP) prevented scale accumulation entirely, maintaining a pristine carbon pore structure and sustaining high desalination performance from the outset.

Mechanistically, these improvements are attributed to the alternating alkaline and acidic microenvironments induced by polarity reversal, where anodic polarization of the former cathode generates localized acidity that dissolves surface-bound carbonate phases and reopens blocked pores.

Overall, this work establishes AP as both a preventive and regenerative operational strategy for mitigating cathodic scaling in CDI systems. By enabling in situ, chemical-free removal of mineral deposits and preserving electrode structure and electrochemical function, AP offers a simple and scalable approach to sustaining initial desalination performance in carbonate-scaling environments. While the long-term impacts of prolonged polarity reversal and the effects of complex, multi-ion real water matrices require further investigation, these short-term findings expand the functional role of AP beyond corrosion mitigation and provide a foundation for its broader application in advanced electrochemical water treatment.

Supplementary Materials: The following supporting information can be downloaded at: https://www.mdpi.com/article/10.3390/w18121513/s1, Figure S1: Scanning electron microscopy (SEM) images of the pristine activated carbon (AC) electrode prior to CDI operation; Figure S2: Energy-dispersive X-ray spectroscopy (EDS) spectra of the cathode electrodes after 16 CDI cycles under three operational modes: (a) conventional cycling, (b) delayed alternating polarization (AP), and (c) immediate AP; Figure S3: Scanning electron microscopy (SEM) images of the anode electrodes after 16 CDI cycles under three operational modes: (a) conventional cycling, (b) delayed alternating polarization (AP), and (c) immediate AP.

Funding: This research was funded by the Ongoing Research Funding program, (ORF-2026-1437), King Saud University, Riyadh, Saudi Arabia.

Data Availability Statement: The original contributions presented in this study are included in the article/Supplementary Materials. Further inquiries can be directed to the author.

Acknowledgments: The author would like to acknowledge the support provided by the Ongoing Research Funding program (ORF-2026-1437), King Saud University, Riyadh, Saudi Arabia. The author confirms that there was no use of artificial intelligence (AI)-assisted technology for assisting in the writing or editing of the manuscript, and no images were manipulated using AI.

Conflicts of Interest: The author declares that he has no known competing financial interests or personal relationships that could have appeared to influence the work reported in this paper.

References

1. Moon, J.; Son, S.; Kim, J.; Park, K. Critical Challenges in High-Salinity Seawater Reverse Osmosis Systems: Technical, Energy, and Environmental Reviews. *Desalination* **2025**, *607*, 118811. [CrossRef]
2. Wu, H.; West, S.R.; Hayward, J.A. Energy Options for Brackish Groundwater Desalination in Western Australia. *Desalination* **2025**, *600*, 118446. [CrossRef]
3. Alenezi, A.; Alabaiadly, Y. Emerging Technologies in Water Desalination: A Review and Future Outlook. *Energy Nexus* **2025**, *17*, 100373. [CrossRef]
4. Pang, T.; Marken, F.; Mattia, D.; Shen, J.; Zhang, D.; Xie, M. Advances and Challenges in Capacitive Deionization: Materials, Architectures, and Selective Ion Removal. *Desalination* **2024**, *592*, 118140. [CrossRef]
5. Alnajdi, S.; Naderi Beni, A.; Alsaati, A.A.; Luhar, M.; Childress, A.E.; Warsinger, D.M. Practical Minimum Energy Use of Seawater Reverse Osmosis. *Joule* **2024**, *8*, 3088–3105. [CrossRef]
6. Patel, S.K.; Biesheuvel, P.M.; Elimelech, M. Energy Consumption of Brackish Water Desalination: Identifying the Sweet Spots for Electrodialysis and Reverse Osmosis. *ACS EST Eng.* **2021**, *1*, 851–864. [CrossRef]
7. Boussouga, Y.-A.; Ramos, R.L.; Ogunniyi, E.O.; Richards, B.S.; Schäfer, A.I. Energy Efficiency of Single-Pass Electrodialysis and Nanofiltration/Reverse Osmosis for Brackish Water Desalination: An Experimental Comparison. *Desalination* **2026**, *621*, 119670. [CrossRef]
8. Orfi, J.; Sherif, R.; AlFaleh, M. Conventional and Emerging Desalination Technologies: Review and Comparative Study from a Sustainability Perspective. *Water* **2025**, *17*, 279. [CrossRef]
9. Tauk, M.; Bechelany, M.; Sistat, P.; Habchi, R.; Cretin, M.; Zaviska, F. Ion-Selectivity Advancements in Capacitive Deionization: A Comprehensive Review. *Desalination* **2024**, *572*, 117146. [CrossRef]
10. He, S.; Zhu, T.; Wang, Y.; Xiong, W.; Gao, X.; Zhang, E. Application of Capacitive Deionization Technology in Water Treatment and Coupling Technology: A Review. *Environ. Sci.* **2024**, *10*, 2313–2340. [CrossRef]
11. Zhao, X.; He, Z.; Li, M.; He, C.; Xu, Y.; Wang, Y.; Ma, J.; Yang, H.Y. Advanced Strategies for Improving the Energy Efficiency of Capacitive Deionization Technologies. *Desalination* **2025**, *597*, 118377. [CrossRef]
12. AL-Rajabi, M.M.; Abumadi, F.A.; Laoui, T.; Atieh, M.A.; Khalil, K.A. Capacitive Deionization for Water Desalination: Cost Analysis, Recent Advances, and Process Optimization. *J. Water Process Eng.* **2024**, *58*, 104816. [CrossRef]
13. Algurainy, Y.; Refaat, A.; Alrehaili, O. Developing Insights into Pretreatment Optimization: Effects of Eliminating Lime and Soda Ash in Groundwater RO Desalination. *Water* **2025**, *17*, 3186. [CrossRef]
14. Salari, K.; Zarafshan, P.; Khashehchi, M.; Chegini, G.; Etezadi, H.; Karami, H.; Szulżyk-Cieplak, J.; Łagód, G. Knowledge and Technology Used in Capacitive Deionization of Water. *Membranes* **2022**, *12*, 459. [CrossRef] [PubMed]
15. Suss, M.E.; Porada, S.; Sun, X.; Biesheuvel, P.M.; Yoon, J.; Presser, V. Water Desalination via Capacitive Deionization: What Is It and What Can We Expect from It? *Energy Environ. Sci.* **2015**, *8*, 2296–2319. [CrossRef]

16. Porada, S.; Zhao, R.; van der Wal, A.; Presser, V.; Biesheuvel, P.M. Review on the Science and Technology of Water Desalination by Capacitive Deionization. *Prog. Mater. Sci.* **2013**, *58*, 1388–1442. [CrossRef]
17. Kong, X.; Zhang, C.; Hou, C.-H.; Waite, T.D.; Ma, J. Fouling in Capacitive Deionization: A Critical Review. *Environ. Sci. Technol.* **2025**, *59*, 13566–13584. [CrossRef] [PubMed]
18. Mossad, M.; Zou, L. Study of Fouling and Scaling in Capacitive Deionisation by Using Dissolved Organic and Inorganic Salts. *J. Hazard. Mater.* **2013**, *244–245*, 387–393. [CrossRef] [PubMed]
19. Chen, T.-H.; Kao, Y.-H.; Shen, Y.-Y.; Fan, C.-S.; Hou, C.-H. Pilot-Scale Membrane Capacitive Deionization for Water Reclamation: Commissioning, Performance Benchmarking, and Long-Term Assessment. *Desalination* **2025**, *599*, 118428. [CrossRef]
20. Algurainy, Y.; Call, D.F. Cathodic Precipitation of Calcium Carbonate and Its Impact on the Electrosorption of Sodium in Flow-through Capacitive Deionization. *Desalination* **2024**, *586*, 117853. [CrossRef]
21. Wang, C.; Chen, L.; Zhu, L. Effect of Combined Fouling on Desalination Performance of Membrane Capacitive Deionization (MCDI) during Long-Term Operation. *J. Dispers. Sci. Technol.* **2020**, *41*, 383–392. [CrossRef]
22. Wang, T.; Zhang, C.; Bai, L.; Xie, B.; Gan, Z.; Xing, J.; Li, G.; Liang, H. Scaling Behavior of Iron in Capacitive Deionization (CDI) System. *Water Res.* **2020**, *171*, 115370. [CrossRef] [PubMed]
23. Zhang, C.; Ma, J.; Wu, L.; Sun, J.; Wang, L.; Li, T.; Waite, T.D. Flow Electrode Capacitive Deionization (FCDI): Recent Developments, Environmental Applications, and Future Perspectives. *Environ. Sci. Technol.* **2021**, *55*, 4243–4267. [CrossRef] [PubMed]
24. Elewa, M.M.; El Batouti, M.; Al-Harby, N.F. A Comparison of Capacitive Deionization and Membrane Capacitive Deionization Using Novel Fabricated Ion Exchange Membranes. *Materials* **2023**, *16*, 4872. [CrossRef] [PubMed]
25. Shapira, B.; Avraham, E.; Aurbach, D. Side Reactions in Capacitive Deionization (CDI) Processes: The Role of Oxygen Reduction. *Electrochim. Acta* **2016**, *220*, 285–295. [CrossRef]
26. Zhang, C.; He, D.; Ma, J.; Tang, W.; Waite, T.D. Faradaic Reactions in Capacitive Deionization (CDI)—Problems and Possibilities: A Review. *Water Res.* **2018**, *128*, 314–330. [CrossRef] [PubMed]
27. Yu, F.; Wang, L.; Wang, Y.; Shen, X.; Cheng, Y.; Ma, J. Faradaic Reactions in Capacitive Deionization for Desalination and Ion Separation. *J. Mater. Chem. A Mater.* **2019**, *7*, 15999–16027. [CrossRef]
28. Algurainy, Y. Enhancing Sodium Removal in Capacitive Deionization via Cathode Asymmetry and Faradaic Reactions Suppression. *J. King Saud Univ. Sci.* **2026**, *38*, 11372025. [CrossRef]
29. Zhang, C.; He, D.; Ma, J.; Tang, W.; Waite, T.D. Comparison of Faradaic Reactions in Flow-through and Flow-by Capacitive Deionization (CDI) Systems. *Electrochim. Acta* **2019**, *299*, 727–735. [CrossRef]
30. Algurainy, Y.; Call, D.F. Asymmetrical Removal of Sodium and Chloride in Flow-through Capacitive Deionization. *Water Res.* **2020**, *183*, 116044. [CrossRef] [PubMed]
31. Yu, J.; Jo, K.; Kim, T.; Lee, J.; Yoon, J. Temporal and Spatial Distribution of PH in Flow-Mode Capacitive Deionization and Membrane Capacitive Deionization. *Desalination* **2018**, *439*, 188–195. [CrossRef]
32. Arulrajan, A.C.; Dykstra, J.E.; Van Der Wal, A.; Porada, S. Unravelling PH Changes in Electrochemical Desalination with Capacitive Deionization. *Environ. Sci. Technol.* **2021**, *55*, 14165–14172. [CrossRef] [PubMed]
33. Kim, C.; Srimuk, P.; Lee, J.; Fleischmann, S.; Aslan, M.; Presser, V. Influence of Pore Structure and Cell Voltage of Activated Carbon Cloth as a Versatile Electrode Material for Capacitive Deionization. *Carbon N. Y.* **2017**, *122*, 329–335. [CrossRef]
34. Luo, L.; Liu, T.; He, J.; Ma, J.; Yu, H.-Q. Ion-Selective Metathesis Design of Flow-Electrode Capacitive Deionization for Energy-Saving and Anti-Scaling Softening of Brackish Water. *Environ. Sci. Technol.* **2024**, *58*, 13120–13130. [CrossRef] [PubMed]
35. Leong, Z.Y.; Yang, H.Y. Capacitive Deionization of Divalent Cations for Water Softening Using Functionalized Carbon Electrodes. *ACS Omega* **2020**, *5*, 2097–2106. [CrossRef] [PubMed]
36. Zeng, Z.-H.; Yan, L.-L.; Li, G.-H.; Rao, P.-H.; Sun, Y.-R.; Zhao, Z.-Y. Development of Biochar Electrode Materials for Capacitive Deionization: Preparation, Performance, Regeneration and Other Challenges. *New Carbon Mater.* **2023**, *38*, 837–860. [CrossRef]
37. Li, M.; Park, H.G. Pseudocapacitive Coating for Effective Capacitive Deionization. *ACS Appl. Mater. Interfaces* **2018**, *10*, 2442–2450. [CrossRef] [PubMed]
38. Kamal, M.S.; Hussein, I.; Mahmoud, M.; Sultan, A.S.; Saad, M.A.S. Oilfield Scale Formation and Chemical Removal: A Review. *J. Pet. Sci. Eng.* **2018**, *171*, 127–139. [CrossRef]
39. Antony, A.; Low, J.H.; Gray, S.; Childress, A.E.; Le-Clech, P.; Leslie, G. Scale Formation and Control in High Pressure Membrane Water Treatment Systems: A Review. *J. Memb. Sci.* **2011**, *383*, 1–16. [CrossRef]
40. Mahima, S.; Kumar, K.S.; Sherugar, P.; Xu, X.; Gurunatha, K.L.; Padaki, M.; Nagaraju, D.H. Impact of Ion Intercalation Materials on Advancing Capacitive Deionization: From Theory to Practical. *Nanoscale Adv.* **2025**, *7*, 4270–4292. [CrossRef] [PubMed]
41. Nnorom, N.C.; Rogers, T.; Jain, A.; Alazmi, A.; Elias, W.C.; DuChanois, R.M.; Flores, K.; Gardea-Torresdey, J.L.; Cokar, M.; Elimelech, M.; et al. Sulfonated Polymer Coating Enhances Selective Removal of Calcium in Membrane Capacitive Deionization. *J. Memb. Sci.* **2022**, *662*, 120974. [CrossRef]
42. Yoon, H.; Lee, J.; Kim, S.-R.; Kang, J.; Kim, S.; Kim, C.; Yoon, J. Capacitive Deionization with Ca-Alginate Coated-Carbon Electrode for Hardness Control. *Desalination* **2016**, *392*, 46–53. [CrossRef]

43. Xiao, Q.; Ma, J.; Xu, L.; Zuo, K.; Guo, H.; Tang, C.Y. Membrane Capacitive Deionization (MCDI) for Selective Ion Separation and Recovery: Fundamentals, Challenges, and Opportunities. *J. Memb. Sci.* **2024**, *699*, 122650. [CrossRef]
44. Gamaethiralalage, J.G.; Singh, K.; Sahin, S.; Yoon, J.; Elimelech, M.; Suss, M.E.; Liang, P.; Biesheuvel, P.M.; Zornitta, R.L.; de Smet, L.C.P.M. Recent Advances in Ion Selectivity with Capacitive Deionization. *Energy Environ. Sci.* **2021**, *14*, 1095–1120. [CrossRef]
45. McNair, R.; Szekely, G.; Dryfe, R.A.W. Ion-Exchange Materials for Membrane Capacitive Deionization. *ACS EST Water* **2021**, *1*, 217–239. [CrossRef]
46. Chen, P.-A.; Lee, K.-T.; Chang, J.-L. A Mini-Review of Ion Exchange Membranes for Capacitive Deionization: Research Progress, Commercialization, and Patent Trends. *Green Energy Fuel Res.* **2025**, *2*, 127–138. [CrossRef]
47. Holubowitch, N.E.; Omosebi, A.; Gao, X.; Landon, J.; Liu, K. Membrane-Free Electrochemical Deoxygenation of Aqueous Solutions Using Symmetric Activated Carbon Electrodes in Flow-through Cells. *Electrochim. Acta* **2019**, *297*, 163–172. [CrossRef]
48. Holubowitch, N.; Omosebi, A.; Gao, X.; Landon, J.; Liu, K. Quasi-Steady-State Polarization Reveals the Interplay of Capacitive and Faradaic Processes in Capacitive Deionization. *ChemElectroChem* **2017**, *4*, 2404–2413. [CrossRef]
49. Lee, B.; Oh, C.; An, J.; Yeon, S.; Oh, H.J. Optimizing Operational Conditions of Pilot-Scale Membrane Capacitive Deionization System. *Sustainability* **2023**, *15*, 16809. [CrossRef]
50. Cuong, D.V. Critical Review of Capacitive Deionization: Design, Operation Consideration and Real-World Environmental Applications. *J. Sci. Technol. Civ. Eng. HUCE* **2024**, *18*, 108–129. [CrossRef] [PubMed]
51. He, D.; Wong, C.E.; Tang, W.; Kovalsky, P.; David Waite, T. Faradaic Reactions in Water Desalination by Batch-Mode Capacitive Deionization. *Environ. Sci. Technol. Lett.* **2016**, *3*, 222–226. [CrossRef]
52. Tang, W.; He, D.; Zhang, C.; Kovalsky, P.; Waite, T.D. Comparison of Faradaic Reactions in Capacitive Deionization (CDI) and Membrane Capacitive Deionization (MCDI) Water Treatment Processes. *Water Res.* **2017**, *120*, 229–237. [CrossRef] [PubMed]
53. Alkhadra, M.A.; Su, X.; Suss, M.E.; Tian, H.; Guyes, E.N.; Shocron, A.N.; Conforti, K.M.; de Souza, J.P.; Kim, N.; Tedesco, M.; et al. Electrochemical Methods for Water Purification, Ion Separations, and Energy Conversion. *Chem. Rev.* **2022**, *122*, 13547–13635. [CrossRef] [PubMed]
54. Gao, X.; Omosebi, A.; Landon, J.; Liu, K. Voltage-Based Stabilization of Microporous Carbon Electrodes for Inverted Capacitive Deionization. *J. Phys. Chem. C* **2018**, *122*, 1158–1168. [CrossRef]
55. Gao, X.; Omosebi, A.; Holubowitch, N.; Landon, J.; Liu, K. Capacitive Deionization Using Alternating Polarization: Effect of Surface Charge on Salt Removal. *Electrochim. Acta* **2017**, *233*, 249–255. [CrossRef]
56. Cohen, I.; Avraham, E.; Bouhadana, Y.; Soffer, A.; Aurbach, D. Electrochimica Acta The Effect of the Fl Ow-Regime, Reversal of Polarization, and Oxygen on the Long Term Stability in Capacitive de-Ionization Processes. *Electrochim. Acta* **2015**, *153*, 106–114. [CrossRef]
57. Remillard, E.M.; Shocron, A.N.; Rahill, J.; Suss, M.E.; Vecitis, C.D. A Direct Comparison of Flow-by and Flow-through Capacitive Deionization. *Desalination* **2018**, *444*, 169–177. [CrossRef]
58. Qu, Y.; Campbell, P.G.; Hemmatifar, A.; Knipe, J.M.; Loeb, C.K.; Reidy, J.J.; Hubert, M.A.; Stadermann, M.; Santiago, J.G. Charging and Transport Dynamics of a Flow-Through Electrode Capacitive Deionization System. *J. Phys. Chem. B* **2018**, *122*, 240–249. [CrossRef] [PubMed]
59. Guyes, E.N.; Shocron, A.N.; Simanovski, A.; Biesheuvel, P.M.; Suss, M.E. A One-Dimensional Model for Water Desalination by Flow-through Electrode Capacitive Deionization. *Desalination* **2017**, *415*, 8–13. [CrossRef]
60. Datar, S.D.; Mane, R.S.; Jha, N. Zeolitic Imidazolate Framework-67 Derived Porous Carbon Electrodes for Efficient Capacitive Deionization. *Appl. Surf. Sci.* **2022**, *604*, 154550. [CrossRef]
61. Kyaw, H.H.; Al-Mashaikhi, S.M.; Myint, M.T.Z.; Al-Harthi, S.; El-Shafey, E.-S.I.; Al-Abri, M. Activated Carbon Derived from the Date Palm Leaflets as Multifunctional Electrodes in Capacitive Deionization System. *Chem. Eng. Process. Process Intensif.* **2021**, *161*, 108311. [CrossRef]
62. Carolina, P.-A.; Roberto, R.-R.; Miguel, O.-S.; David, S.G.-G.; Rene, R.-M.; Luis, F.C.-R.; Miguel, A.-B.; Javier, A.A.-O. N-Doped Activated Carbons from Leather Waste Produced by Microwave Activation for Use as the Cathode of Li-S Batteries. *New Carbon Mater.* **2025**, *40*, 382–395. [CrossRef]
63. Zhang, X.; Zuo, K.; Zhang, X.; Zhang, C.; Liang, P. Selective Ion Separation by Capacitive Deionization (CDI) Based Technologies: A State-of-the-Art Review. *Environ. Sci.* **2020**, *6*, 243–257. [CrossRef]
64. Huang, Z.H.; Yang, Z.; Kang, F.; Inagaki, M. Carbon Electrodes for Capacitive Deionization. *J. Mater. Chem. A Mater.* **2017**, *5*, 470–496. [CrossRef]
65. Qu, Y.; Baumann, T.F.; Santiago, J.G.; Stadermann, M. Characterization of Resistances of a Capacitive Deionization System. *Environ. Sci. Technol.* **2015**, *49*, 9699–9706. [CrossRef] [PubMed]
66. Kim, J.S.; Choi, J.H. Fabrication and Characterization of a Carbon Electrode Coated with Cation-Exchange Polymer for the Membrane Capacitive Deionization Applications. *J. Memb. Sci.* **2010**, *355*, 85–90. [CrossRef]
67. Ramadan, M.; Hassan, H.M.A.; Shahat, A.; Elshaarawy, R.F.M.; Allam, N.K. Ultrahigh Performance of Novel Energy-Efficient Capacitive Deionization Electrodes Based on 3D Nanotubular Composites. *New J. Chem.* **2018**, *42*, 3560–3567. [CrossRef]

68. Uwayid, R.; Seraphim, N.M.; Guyes, E.N.; Eisenberg, D.; Suss, M.E. Characterizing and Mitigating the Degradation of Oxidized Cathodes during Capacitive Deionization Cycling. *Carbon N. Y.* **2021**, *173*, 1105–1114. [CrossRef]
69. Srimuk, P.; Kaasik, F.; Krüner, B.; Tolosa, A.; Fleischmann, S.; Jäckel, N.; Tekeli, M.C.; Aslan, M.; Suss, M.E.; Presser, V. MXene as a Novel Intercalation-Type Pseudocapacitive Cathode and Anode for Capacitive Deionization. *J. Mater. Chem. A Mater.* **2016**, *4*, 18265–18271. [CrossRef]
70. Zhang, Y.; Ren, P.; Liu, Y.; Presser, V. Particle Size Distribution Influence on Capacitive Deionization: Insights for Electrode Preparation. *Desalination* **2022**, *525*, 115503. [CrossRef]
71. Zhang, Y.; Ren, P.; Wang, L.; Pameté, E.; Husmann, S.; Presser, V. Selectivity toward Heavier Monovalent Cations of Carbon Ultramicropores Used for Capacitive Deionization. *Desalination* **2022**, *542*, 116053. [CrossRef]
72. Gong, C.; Chen, Z.; Geng, W.; Fu, Z.; Chen, C.; Zhang, Y.; Wang, G. Controlled Fabrication of Nitrogen-Doped Porous Carbon Foam with Refined Hierarchical Architectures for Desalination via Capacitive Deionization. *J. Colloid Interface Sci.* **2023**, *643*, 516–527. [CrossRef] [PubMed]
73. Ren, P.; Wang, B.; de Andrade Ruthes, J.G.; Torkamanzadeh, M.; Presser, V. Cation Selectivity during Flow Electrode Capacitive Deionization. *Desalination* **2024**, *592*, 118161. [CrossRef]
74. Ren, P.; Torkamanzadeh, M.; Zhang, X.; Twardoch, M.; Kim, C.; Presser, V. Conductive Carbon Additives: Friend or Foe of Capacitive Deionization with Activated Carbon? *Carbon N. Y.* **2023**, *213*, 118191. [CrossRef]
75. Hassanvand, A.; Chen, G.Q.; Webley, P.A.; Kentish, S.E. A Comparison of Multicomponent Electrosorption in Capacitive Deionization and Membrane Capacitive Deionization. *Water Res.* **2018**, *131*, 100–109. [CrossRef] [PubMed]
76. Choi, J.; Dorji, P.; Shon, H.K.; Hong, S. Applications of Capacitive Deionization: Desalination, Softening, Selective Removal, and Energy Efficiency. *Desalination* **2019**, *449*, 118–130. [CrossRef]
77. Gao, X.; Omosebi, A.; Ma, Z.; Zhu, F.; Landon, J.; Ghorbanian, M.; Kern, N.; Liu, K. Capacitive Deionization Using Symmetric Carbon Electrode Pairs. *Environ. Sci.* **2019**, *5*, 660–671. [CrossRef]
78. Liu, P.; Yan, T.; Shi, L.; Park, H.S.; Chen, X.; Zhao, Z.; Zhang, D. Graphene-Based Materials for Capacitive Deionization. *J. Mater. Chem. A Mater.* **2017**, *5*, 13907–13943. [CrossRef]
79. Jin, H.; Yu, Y.; Zhang, L.; Yan, R.; Chen, X. Polarity Reversal Electrochemical Process for Water Softening. *Sep. Purif. Technol.* **2019**, *210*, 943–949. [CrossRef]
80. Landon, J.; Gao, X.; Omosebi, A.; Liu, K. Emerging Investigator Series: Local PH Effects on Carbon Oxidation in Capacitive Deionization Architectures. *Environ. Sci.* **2021**, *7*, 861–869. [CrossRef]
81. Algurainy, Y.; Call, D.F. Improving Long-Term Anode Stability in Capacitive Deionization Using Asymmetric Electrode Mass Ratios. *ACS ES T Eng.* **2022**, *2*, 129–139. [CrossRef]
82. Jaramillo, J.; Modesto, P.; Gómez-serrano, V. Oxidation of Activated Carbon by Dry and Wet Methods Surface Chemistry and Textural Modi Fi Cations. *Fuel Process. Technol.* **2010**, *91*, 1768–1775. [CrossRef]
83. Berenguer, R.; Morallón, E. Oxidation of Different Microporous Carbons by Chemical and Electrochemical Methods. *Front. Mater.* **2019**, *6*, 130. [CrossRef]
84. Imai, H.; Terada, T.; Miura, T.; Yamabi, S. Self-Organized Formation of Porous Aragonite with Silicate. *J. Cryst. Growth* **2002**, *244*, 200–205. [CrossRef]
85. Ni, M.; Ratner, B.D. Differentiating Calcium Carbonate Polymorphs by Surface Analysis Techniques—An XPS and TOF-SIMS Study. *Surf. Interface Anal.* **2008**, *40*, 1356–1361. [CrossRef] [PubMed]
86. Zafra, M.C.; Lavela, P.; Macías, C.; Rasines, G.; Tirado, J.L. Electrosorption of Environmental Concerning Anions on a Highly Porous Carbon Aerogel. *J. Electroanal. Chem.* **2013**, *708*, 80–86. [CrossRef]
87. Mei, B.A.; Munteshari, O.; Lau, J.; Dunn, B.; Pilon, L. Physical Interpretations of Nyquist Plots for EDLC Electrodes and Devices. *J. Phys. Chem. C* **2018**, *122*, 194–206. [CrossRef]
88. Bouhadana, Y.; Avraham, E.; Noked, M.; Ben-Tzion, M.; Soffer, A.; Aurbach, D. Capacitive Deionization of NaCl Solutions at Non-Steady-State Conditions: Inversion Functionality of the Carbon Electrodes. *J. Phys. Chem. C* **2011**, *115*, 16567–16573. [CrossRef]
89. Sedighi, M.; Behvand Usefi, M.M.; Ismail, A.F.; Ghasemi, M. Environmental Sustainability and Ions Removal through Electrodialysis Desalination: Operating Conditions and Process Parameters. *Desalination* **2023**, *549*, 116319. [CrossRef]
90. Zhao, D.; Yu, S. A Review of Recent Advance in Fouling Mitigation of NF/RO Membranes in Water Treatment: Pretreatment, Membrane Modification, and Chemical Cleaning. *Desalination Water Treat.* **2015**, *55*, 870–891. [CrossRef]
91. Gul, A.; Hruza, J.; Yalcinkaya, F. Fouling and Chemical Cleaning of Microfiltration Membranes: A Mini-Review. *Polymers* **2021**, *13*, 846. [CrossRef] [PubMed]
92. Simbeye, C.; Courtney, C.; Simha, P.; Fischer, N.; Randall, D.G. Human Urine: A Novel Source of Phosphorus for Vivianite Production. *Sci. Total Environ.* **2023**, *892*, 164517. [CrossRef] [PubMed]

93. Lei, Y.; Saakes, M.; van der Weijden, R.D.; Buisman, C.J.N. Electrochemically Mediated Calcium Phosphate Precipitation from Phosphonates: Implications on Phosphorus Recovery from Non-Orthophosphate. *Water Res.* **2020**, *169*, 115206. [CrossRef] [PubMed]
94. Lei, Y.; Song, B.; Saakes, M.; van der Weijden, R.D.; Buisman, C.J.N. Interaction of Calcium, Phosphorus and Natural Organic Matter in Electrochemical Recovery of Phosphate. *Water Res.* **2018**, *142*, 10–17. [CrossRef] [PubMed]
95. Ray, H.; Saetta, D.; Boyer, T.H. Characterization of Urea Hydrolysis in Fresh Human Urine and Inhibition by Chemical Addition. *Environ. Sci.* **2018**, *4*, 87–98. [CrossRef]
96. Mihelcic, J.R.; Fry, L.M.; Shaw, R. Global Potential of Phosphorus Recovery from Human Urine and Feces. *Chemosphere* **2011**, *84*, 832–839. [CrossRef] [PubMed]

Disclaimer/Publisher's Note: The statements, opinions and data contained in all publications are solely those of the individual author(s) and contributor(s) and not of MDPI and/or the editor(s). MDPI and/or the editor(s) disclaim responsibility for any injury to people or property resulting from any ideas, methods, instructions or products referred to in the content.